PCCP

PAPER

View Article Online
View Journal | View Issue

Published on 03 September 2015. Downloaded by Michigan State University on 19/01/2016 16:58:04.

Cite this: *Phys. Chem. Chem. Phys.*, 2015, **17**, 25583

Exponential size-dependent tunability of strain on the transport behavior in ZnO tunnel junctions: an *ab initio* study†

Jia Zhu,[ab] W. J. Chen,[abd] G. H. Zhang[ab] and Yue Zheng*[abc]

Received 7th July 2015,
Accepted 3rd September 2015

DOI: 10.1039/c5cp03945b

www.rsc.org/pccp

It is an interesting issue if the transport behavior of a piezoelectric tunnel junction is sensitive to external strain or stress, and it implies a prospect for developing novel mechanical sensors, transducers, piezotronic devices, *etc.* Many studies paid attention to this issue, yet how the strain and stress tunable transport behavior of a tunnel junction depends on the barrier thickness is still rarely known. Using the first principles calculations, we investigate the size-dependent and strain-tunable transport behavior in the tunnel junctions. It was confirmed that external strain has strong control over the transport properties of ZnO tunnel junctions, with several times amplification of tunnel conductance obtained by strain reversal. More importantly, the conductance amplification by strain reversal exponentially changes with the barrier thickness, indicating the size-dependent strain tunability of the transport behavior. The electrostatic quantities (*i.e.*, built-in field, depolarization field, polarization, interfacial dipoles and potential barrier) and the transport properties of tunnel junctions were comprehensively analyzed to reveal the relationships between these quantities and their size dependence. The exponential size-dependence of strain tunable transport behavior in ZnO tunnel junctions is attributed to the linear change in the potential barrier with the barrier thickness. Our simulations provide an insight of how to maximize the strain tunability of transport behavior of piezoelectric tunnel junctions by thickness design and strain engineering.

1 Introduction

During the past decades, a lot of novel functional nanosystems (*e.g.*, ferroelectric or piezoelectric sensors, actuators and energy harvesters) based on their large strain or stress tunability have been exploited to show extraordinary performance.[1–6] Recently, a new field of piezotronics has emerged, and the transport characteristics of piezoelectric semiconductors can be tuned by piezoelectric polarization switching under externally applied strain.[4,6] Particularly, the tunnel conductance of ferroelectric or piezoelectric tunnel junctions (FTJs or PTJs), *i.e.*, the ultrathin ferroelectric or piezoelectric barrier (<10 nm), has also been found to be significantly tuned by external strain or stress, which has been named as the giant piezoelectric resistance effect.[7–9] This is due to the fact that the polarization state of the ferroelectric or piezoelectric barrier is sensitive to external strain or stress (*e.g.*, *via* piezoelectric and electrostrictive effects), and consequently the potential barrier is affected by the magnitude of the polarization. For example, it has been shown that the conductance of Pt/$PbTiO_3$/Pt FTJ decreases tremendously as the in-plane strain changes from the tensile to compressive state.[8] Meanwhile, the tunnel current of Ag/ZnO/Ag and Au/GaN/Au PTJs is found to change several orders of magnitude under in-plane strain.[9] These studies imply the prospect of FTJs and PTJs in novel strain-tuning electronic devices such as mechanical sensors and transducers.

From the viewpoint of classical quantum tunneling theory, barrier thickness is crucial for a tunnel junction (TJ) to show an obvious tunnel current. For a simple dielectric TJ (*i.e.*, neither ferroelectric nor piezoelectric), its tunnel conductance is expected to change with the barrier thickness in an exponential law. In this case, the barrier thickness affects the potential barrier width in a linear way. The scenario, however, should be more complicated for FTJs and PTJs, considering the additional dependence of polarization on barrier thickness. On the one hand, as the importance of the depolarization field effect increases with the decrease of barrier thickness, the barrier polarization state in FTJs and PTJs is influenced by the barrier thickness.[10–14]

[a] *State Key Laboratory of Optoelectronic Materials and Technologies, School of Physics and Engineering, Sun Yat-sen University, Guangzhou, 510275, China. E-mail: zhengy35@mail.sysu.edu.cn; Tel: +86 8411-3231*
[b] *Micro&Nano Physics and Mechanics Research Laboratory, School of Physics and Engineering, Sun Yat-sen University, Guangzhou, 510275, China*
[c] *Departments of Mechanical Engineering and Civil and Environmental Engineering, Northwestern University, Evanston, IL 60208, USA*
[d] *Sino-French Institute of Nuclear Engineering and Technology, Sun Yat-sen University, Zhuhai, 519082, China*

† Electronic supplementary information (ESI) available. See DOI: 10.1039/c5cp03945b

Published on 03 September 2015. Downloaded by Michigan State University on 19/01/2016 16:58:04.

Actually, this is the main reason why the polarization stability of FTJs is likely to have a critical thickness, and why thinner piezoelectric films usually exhibit a smaller spontaneous polarization. On the other hand, besides the depolarization effect, in asymmetric FTJs and PTJs the built-in field is also found to be important in determining the overall size dependence of polarization. Such a field breaks the degeneracy of the polarization states opposite to the out-of-plane direction.[11,14–16] Specifically, the stability of the polarization state in the same (opposite) direction with the built-in field is enhanced (suppressed), respectively. As the built-in field is a function of the barrier thickness, the dependence of polarization stability on the barrier thickness in asymmetric FTJs and PTJs is further modified by this effect, as has been verified in FTJs.[10,16]

Due to the nonlinear size dependence of polarization, the tunnel conductance of FTJs and PTJs is likely to change with the barrier thickness in a non-exponential law. In literature, size-dependent tunnel conductance in a specific kind of asymmetric FTJ has been revealed, and one can note that the tunnel conductance *versus* barrier thickness curves deviate from the exponential law when the barrier thickness is small enough (near critical thickness).[17] Despite the results of this work, how the electronic transport characteristic of a FTJ or PTJ depends on the barrier thickness is still a rarely known issue. Moreover, considering that strain simultaneously tunes the polarization in FTJs and PTJs, the strain tunability of the potential barrier and thus tunnel conductance in FTJs and PTJs is believed to be further modified by barrier thickness. Exploring the size-dependence of strain tunability is vital for the application of FTJs and PTJs in strain-tuning electronic devices, which however has seldom been investigated to the best of our knowledge.

With the aim of filling the blank in the knowledge of this issue, in this paper, we employed the first principles calculations combined with the nonequilibrium Green's function (NEGF) method[18] to figure out the size-dependence of tunability of strain on the transport behavior in Au/ZnO/Au piezoelectric tunnel junctions with an ultrathin ZnO barrier and asymmetric interfaces. From a theoretical point of view, two major effects should be figured out in order to clarify this issue (as shown in Fig. 1). First, the difference in the work function steps at Au/Zn and O/Au interfaces introduces a built-in field,[16] meanwhile the incomplete screening of the polarization charges by the electrodes leads to a depolarization field.[14,19] How these fields and thus other electrostatic quantities (such as the polarization and potential barrier) scale with the ZnO barrier thickness? Second, strain on the one hand affects the polarization of the ZnO ultrathin barrier (consequently the depolarization field) *via* the piezoelectric effect, and on the other hand possibly modifies the work function steps at two interfaces and thus the built-in field. How strain further modifies the barrier thickness dependence of the polarization and potential barrier? After figuring out these two effects, the strain-tunability of the transmission probability and tunnel conductance of ZnO PTJs with different ZnO barrier thicknesses is further revealed. The size-dependence of strain-tunability on the transport behavior of ZnO PTJs is explained by the WKB model.[20,21]

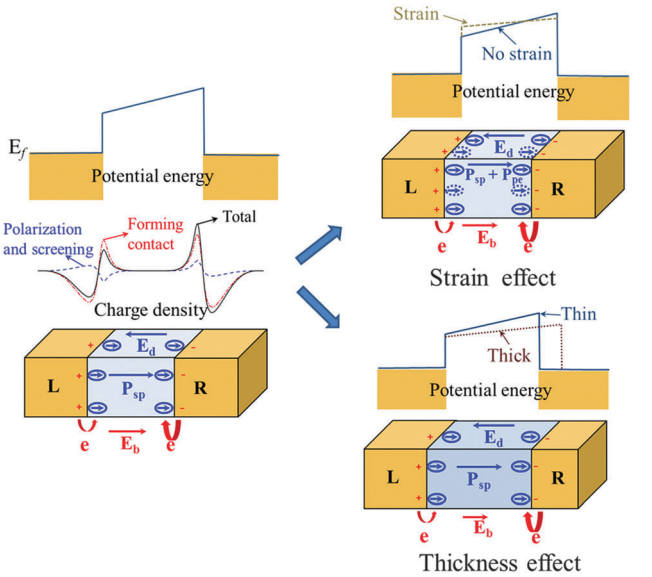

Fig. 1 Schematic of the electronic structure of ZnO PTJs (including the polarization, deformation charge density and electrostatic potential energy). In particular, the possible impact of strain and barrier thickness on the electrostatic properties of ZnO PTJs (*e.g.*, the built-in field, polarization and electrostatic potential energy) is illustrated.

2 Simulation model and method

A typical PTJ structure is schematically shown in Fig. 2(a), where a supercell with a ZnO barrier sandwiched by Au electrodes is built. The ZnO barrier is (0001) orientated and has two polar surfaces, namely, the Zn-surface and the O-surface. The Au electrodes are (111) cleaved to match the hexagonal stacking pattern of the ZnO barrier. Considering that Au electrodes have better ductility, the in-plane lattice constants of the supercell free of external strain are set as the theoretical value of bulk ZnO ($\sim$3.28 Å). The right and left electrodes are 11 and 10 layers thick, respectively, to ensure that the interior Au atoms recover the properties of their bulk counterpart, which is crucial for accurately calculating the transport behavior of ZnO PTJs. As shown in Fig. 2(b), the FTJ systems are constructed with the interfacial ZnO layers (Zn or O layer atoms) occupying either the top ('t') or hollow ('h') site of the interfacial Au atoms. This is because the ZnO PTJs with interfacial atoms occupying the 't' and 'h' sites have the lowest interfacial energy according to our calculations, which is also in agreement with former calculations on the metal/semiconductor contact.[8,9] Considering that the PTJ has two interfaces, namely, the Au/Zn (left) interface and the O/Au (right) interface, we built four supercells with different interfacial bonding structures and denoted them 'h_h', 'h_t', 't_t' and 't_h' PTJs. For example, for 'h_t' PTJs, Zn atoms occupy the hollow site of Au atoms at the Au/Zn interface whereas O atoms occupy the top site of Au atoms at the O/Au interface. The barrier thickness is characterized by the stacking number of ZnO unit cells *m*.

In order to obtain the ground state of ZnO PTJs, we employ density functional theory (DFT) calculations implemented in the Vienna Ab Initio Simulation Package (VASP).[22] We adopt a

 This journal is © the Owner Societies 2015

Published on 03 September 2015. Downloaded by Michigan State University on 19/01/2016 16:58:04.

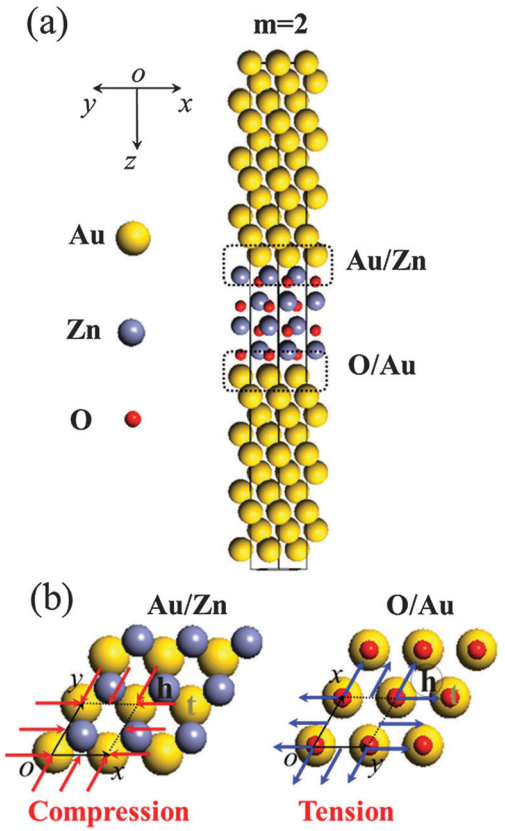

Fig. 2 (a) Atomic structure of the 'h_t' PTJ with m = 2. (b) The interfacial structure of the ZnO PTJ and a schematic diagram of in-plain strain (compression and tension) indicated by arrows. 'h' and 't' stand for the hollow and top sites, respectively.

plane-wave basis set together with the projector augmented wave (PAW)[23] method within the generalized gradient approximation (GGA)[24] and additional on-site Coulomb interaction (U).[25] We set the Hubbard U correction to 12 and 6.5 for O 2p and Zn 3d orbitals in order to open up the band gap of ZnO.[26–29] This is very important to correctly describe the ZnO/Au contact (see the Discussion in the following). A 13 × 13 × 1 Monkhorst–Pack grid for k-point sampling and a 0.1 eV Gaussian broadening are used during relaxation. The positions of ions and the out-of-plane lattice constant are fully optimized until the energy difference is less than 10^{-5} eV and the Hellman–Feynman force acting on each ion is less than 0.01 eV Å^{-1}. Following that, static calculations are performed to obtain the free energy, deformation charge density and electrostatic potential energy of the optimized supercells. In particular, the cohesion energies of the four kinds of PTJs are calculated using,[8,30,31]

$$W_{co} = (E_{ZnO} + E_{Au} - E_{Au-ZnO-Au})/2A \quad (1)$$

where $E_{Au-ZnO-Au}$ is the free energy of optimized supercells, and E_{ZnO} and E_{Au} are the energies of the same supercell containing only ZnO and Au component slabs, respectively, A is the area of the interface and factor 2 represents two interfaces.

Then, in-plane strain (compression and tension) is loaded on the supercells with different barrier thicknesses (m ranging from 2 to 7) to study the size-dependence of strain tunability on its potential barrier. Furthermore, these supercells are used to construct two-probe systems (*i.e.*, ZnO PTJs) in the Atomistix ToolKit (ATK) package. It is assumed that the two-probe structure is periodic in the x–y plane with two semi-infinite electrodes and a barrier. Based on the NEGF method, a numerical atomic-orbital basis set of double ζ plus polarization (DZP) is used for all atoms to ensure high accuracy of calculations. The exchange correlation pseudo-potential with Perdew–Burke–Ernzerhof (PBE) parameterization of GGA combined with on-site Coulomb interaction (U) is adopted to be consistent with former calculations. A dense Monkhorst–Pack grid of 18 × 18 × 100 in k-point sampling is adopted to obtain the self-consistent charge density, and a 70 × 70 mesh in two-dimensional Brillouin zone is used to calculate the transmission probability and the tunnel conductance of ZnO PTJs. Importantly, the size-dependence of strain-tunability on the tunnel conductance of ZnO PTJs is revealed, and we provide an analysis in the framework of the classical WKB model.

3 Results and discussion

3.1 The deformation charge density and the electrostatic potential energy

It is found that the 'h_t' system is the most energetically stable due to its strongest cohesion energy (see the Table 1), which results from the best bonding at both the O/Au and Au/Zn interfaces. Also note that the difference in cohesion energies between the 'h_h' and 'h_t' systems (∼0.02308 eV Å^{-2}) is larger than that between the 't_t' and 'h_t' systems (∼0.02130 eV Å^{-2}), indicating that the cohesion energy of the O/Au interface dominates for the whole 'h_t' system. By studying the deformation charge density $\rho_{scf-nscf}$ (the difference in charge densities between those obtained from a self-consistent calculation and a non-self-consistent calculation (*i.e.*, a superposition of atomic electron charge densities in our case), *i.e.*, $\rho_{scf} - \rho_{nscf}$) on the (110) plane, as shown in Fig. 3(a), one can see that Zn atoms occupying the hollow site of Au atoms at the Au/Zn interface avails the bonding between Au and O atoms due to the short distance between them. Meanwhile, O atoms prefer to sit atop Au atoms at the O/Au interface to form a tetrahedral bonding structure, which is consistent with former calculations on semiconductor/metal contacts.[32]

Furthermore, we calculated the macro-average of the deformation charge density and the electrostatic potential energy along the z-axis using a double-macro average method.[8,14,33] This method filters the periodic fluctuation of the charge density and the potential energy, which is useful for analyzing the interface. Take the deformation charge density for example. The macro-average of deformation charge density along the

Table 1 The cohesion energies of four ZnO PTJs with different interfacial structures

Structures	h_h	h_t	t_t	t_h
W_{co} (eV Å^{-2})	0.07114	0.09422	0.08324	0.06194

Published on 03 September 2015. Downloaded by Michigan State University on 19/01/2016 16:58:04.

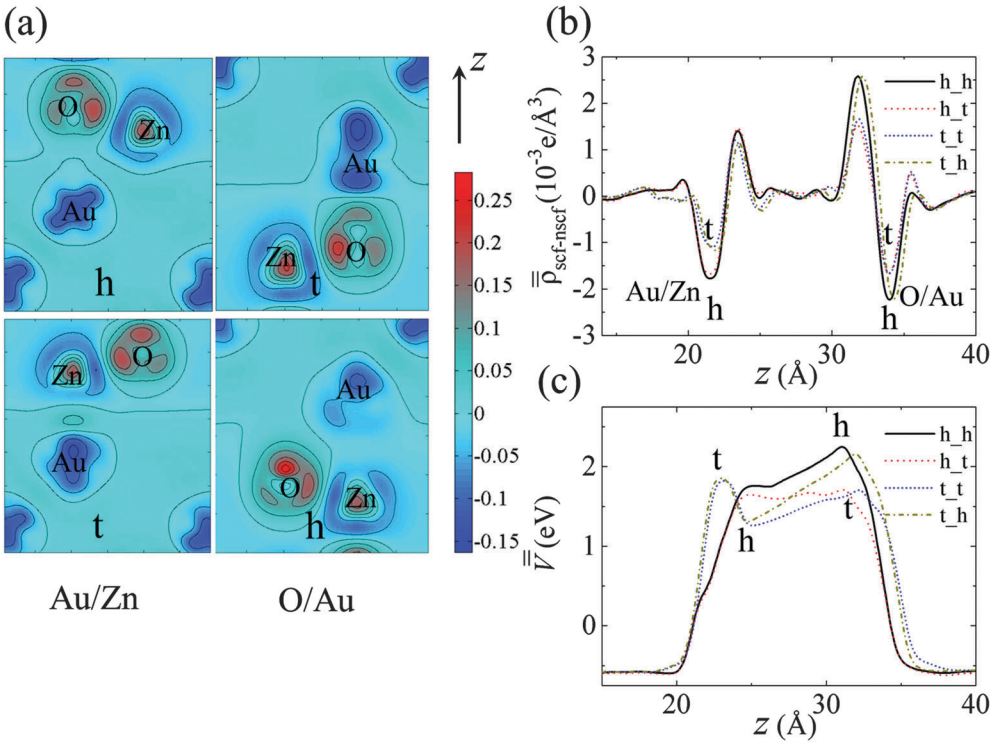

Fig. 3 (a) The deformation charge density on the (110) plane of different interfacial structures. The macro-average of deformation charge density (b) and electrostatic potential energy (c) along the z-axis of ZnO PTJs with different interfacial structures.

z-axis is given by $\overline{\overline{\rho}}_{\mathrm{scf-nscf}}(z) = \int_{z-L}^{z+L} \mathrm{d}z' f(z-z') \overline{\rho}_{\mathrm{scf-nscf}}(z')$, where $\overline{\rho}_{\mathrm{scf-nscf}}(z')$ is the deformation charge density averaged along the xy-plane and L is the z-lattice constant of Au or ZnO unit cells. $f(z–z')$ is a smoothing function which is a convolution of two square-wave filter functions in our case. Two interfacial dipoles with opposite signs are clearly shown in Fig. 3(b), and their magnitudes depend on the respective interfacial structures. For example, the PTJ with a 'h' structure at the Au/Zn interface corresponds to a larger interfacial dipole than that with a 't' structure. This is mainly due to the better bonding between Au and O atoms in the 'h' structure. It is also observed that the magnitude of a specific interfacial dipole in different types of PTJs is quite similar, indicating the well-kept local features of the specific interfaces in different types of PTJs. It should be pointed out that the interfacial dipoles result from two contributions (as illustrated in Fig. 1), *i.e.*, the charge transfer during the formation of Schottky barriers;[34,35] secondly, the spontaneous polarization of the ZnO barrier and the screening effect of electrodes.[11,14,19] Consequently, the electric field in the ZnO barrier region is also composed of two contributions, *i.e.*, the built-in field introduced by different charge transfers during the formation of Schottky barriers at the two interfaces, and secondly, the depolarization field due to the spontaneous polarization of the ZnO barrier and the imperfect screening of Au electrodes. By analyzing the macro-averaged electrostatic potential energy ($\overline{\overline{V}}$, shown in Fig. 3(c)), one can see that the electric field in the ZnO barrier precisely relies on the difference between the Au/Zn and O/Au interfacial dipoles. For example, the 't_h' PTJ has the largest difference in interfacial dipoles, thus it corresponds to the largest electric field in the ZnO barrier (see the olive dashed dotted line).

3.2 The size-dependent electrostatic potential energy

We built supercells with different ZnO barrier thicknesses (*i.e.*, m ranging from 2 to 5) based on the most energetically stable ('h_t') and unstable ('t_h') PTJ systems to investigate the impact of the barrier thickness on the polarization. As shown in Fig. 4(a) and (b), for both types of PTJs at various thicknesses, the total electric field in the ZnO barrier is along the positive direction. This direction is just the direction of the built-in field (from Au/Zn to O/Au interface), since the depolarization field is along the negative direction due to the calculated positive spontaneous polarization in the ZnO barrier. This indicates that the built-in field dominates over the depolarization field in both types of PTJs. The deformation charge density on the (110) plane of 'h_t' PTJs with m ranging from 2 to 5 is shown in Fig. S1 (ESI†). It is found that the charge transfer almost does not change with m, which implies that the interfacial dipole has no obvious dependence on the ZnO barrier thickness. Moreover, the electric field in the barrier increases with the decrease of barrier thickness m in both types of PTJs, which is consistent with thermodynamic models[10,16] and other first principles calculations.[36,37]

Table 2 gives the local spontaneous polarization of each ZnO unit cell along the z-axis in the 'h_t' supercell with respect to m

 This journal is © the Owner Societies 2015

Published on 03 September 2015. Downloaded by Michigan State University on 19/01/2016 16:58:04.

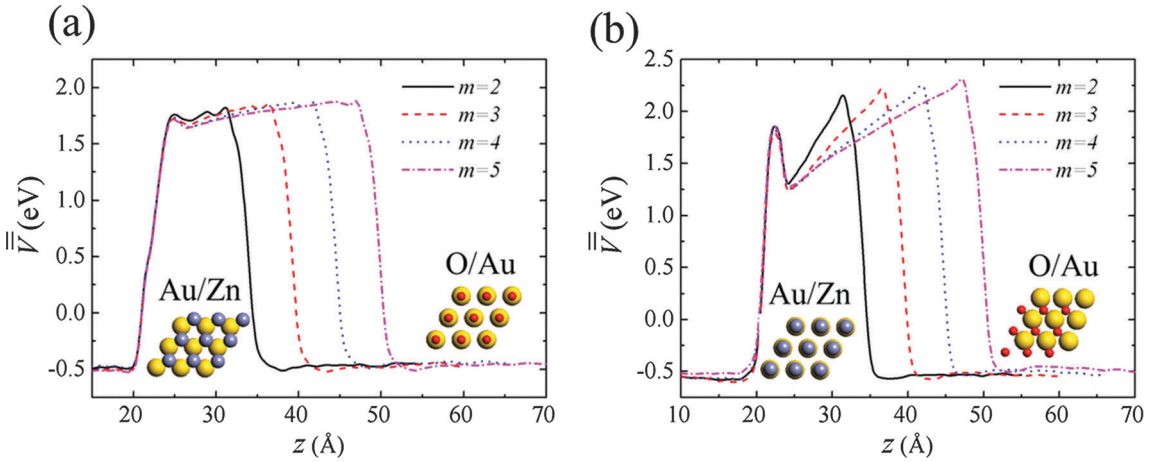

Fig. 4 The macro-average of electrostatic potential energy of 'h_t' (a) and 't_h' (b) ZnO PTJ with different m (from 2 to 5). The inset shows the details of their interfacial structures.

Table 2 The polarization (in unit of C m^{-2}) of each ZnO unit cell from the left (index '1', in bold) to right (in italics) interface in 'h_t' ZnO PTJs with different m (from 2 to 5) under zero strain. The sign '±' denotes the polarization pointing from the Au/Zn to O/Au interface and the reverse, respectively

m				
Index	2	3	4	5
1	**−0.008705**	**−0.014213**	**−0.01288**	**−0.014935**
2	*0.0963*	0.0552	0.05561	0.05358
3		*0.08187*	0.05346	0.05142
4			*0.08467*	0.04953
5				*−0.07579*

obtained by the Born effective charge method.[38] It is found that the spontaneous polarization is almost uniform in the barrier except near the two interfaces (see the italics and bold regions in Table 2). Most importantly, the average spontaneous polarization of central ZnO unit cells (except those at the interfaces) in each supercell is always larger than its bulk level (∼0.04 C m^{-2}), and meanwhile it decreases slightly with the increase of m. When m equals 5, the average spontaneous polarization of central ZnO unit cells (∼0.05 C m^{-2}) approaches its bulk level. Obviously, the spontaneous polarization is enhanced by the built-in field due to their same direction, which is similar to the case of FTJs.[11,16] With the increase of m, this enhancement is weakened due to the smaller built-in field.

3.3 Strain controlling electrostatic potential energies with different barrier thicknesses

The 'h_t' PTJs with different barrier thicknesses m under in-plane strain are investigated. As shown in Fig. 5(a)–(c), the electric field under −3% strain is always larger than that under 3% strain. This can be understood from the fact that the electric field of the 'h_t' system free of strain is along the positive direction (see Fig. 4(a)), meanwhile the depolarization field associated with strain-induced (*i.e.*, piezoelectric) polarization under −3% (3%) strain is along the positive (negative) direction. Importantly, calculations pointed out that the built-in field may also be modified by the strain. Nevertheless, as the piezoelectric polarization is quite large (see Tables 3 and 4), it is difficult to separately quantify the built-in field effect from the depolarization effect. The impact of strain on the electric potential energy and thus the electric field of ZnO PTJs originates from its tunability of the electronic structure. As shown in Fig. S2 (ESI†), the in-plane strain can effectively tune the interfacial charge transfer. Generally speaking, in-plane compressive strain corresponds to larger interfacial dipoles. Also note that the change in the electric field from −3% to 3% strain decreases with the increase of m, indicating a better strain tunability of the electric field when the ZnO barrier is relatively thinner. This is as expected since both the built-in field and the depolarization field are inversely proportional to the barrier thickness. When m equals 6, the values of the electric field of the barrier region under −3% and 3% strain are very close (shown in Fig. 5(c)). It is also observed that PTJs under 3% strain always have a lower potential barrier than those under −3% strain, and the difference in potential energies between 3% and −3% strain decreases with ZnO barrier thickness (see the 'ΔV' in Fig. 5(a)–(c)). Additionally, the difference in the potential barrier width between 3% and −3% strain increases with the increase of m (see the 'Δd' in Fig. 5(a)–(c)) because the ZnO layer extends (shortens) under in-plane compression (tensile) strain.

Furthermore, the total polarization (sum of spontaneous and piezoelectric polarization) of the strained 'h_t' PTJs is also calculated (see Tables 3 and 4 for PTJs under 3% and −3% strain, respectively). Under 3% tensile strain, the total polarization of the PTJ is strengthened since the piezoelectric polarization under tension is in the same direction with spontaneous polarization. Meanwhile, the total polarization of ZnO unit cells in the middle of the supercell is larger than that of bulk ZnO under same strain (∼0.17 C m^{-2}) due to the impact of the built-in field. In contrast, for the PTJs under −3% compressive strain, the direction of the total polarization is reversed by opposite piezoelectric polarization. The polarization of ZnO unit cells in the central barrier region is smaller than that of bulk ZnO under same strain (∼−0.12 C m^{-2})

Published on 03 September 2015. Downloaded by Michigan State University on 19/01/2016 16:58:04.

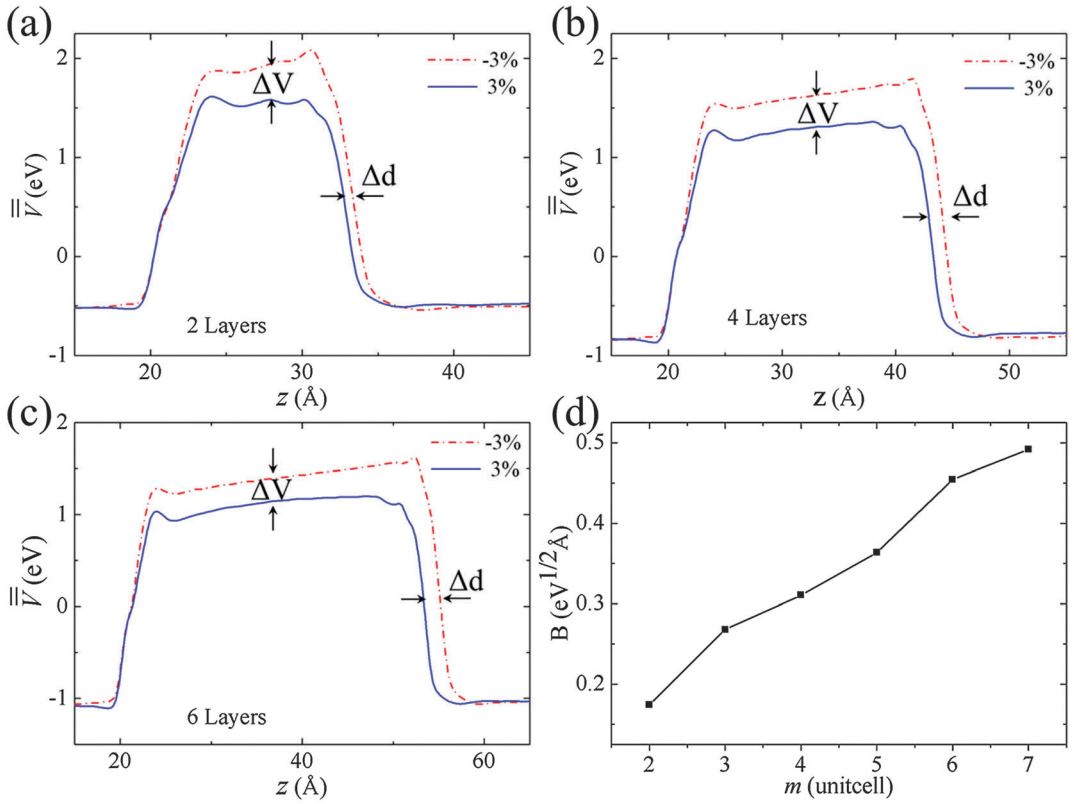

Fig. 5 (a–c) The macro-average of electrostatic potential energy of the 'h_t' ZnO PTJs with different m (2, 4 and 6) under ±3% in-plane strain. The change in the potential barrier by strain reversal is denoted by the shade area. 'ΔV' and 'Δd' indicate the difference in the potential barrier height and width by strain reversal. (d) The parameter B (see the main part for definition) scaling with m.

Table 3 The polarization (in units of C m^{-2}) of each ZnO unit cell from the left (index '1', in bold) to right (in italics) interface in 'h_t' ZnO PTJs with different m (from 2 to 5) under 3% strain

m				
Index	2	3	4	5
1	**0.13105**	**0.11966**	**0.1209**	**0.11761**
2	*0.23906*	0.23775	0.19249	0.18981
3		*0.22438*	0.18885	0.18116
4			*0.21514*	0.17854
5				*0.21086*

Table 4 The polarization (in units of C m^{-2}) of each ZnO unit cell from the left (index '1', in bold) to right (in italics) interface in 'h_t' ZnO PTJs with different m (from 2 to 5) under −3% strain

m				
Index	2	3	4	5
1	**−0.159496**	**−0.165047**	**−0.168002**	**−0.167635**
2	*−0.07322*	−0.105982	−0.107315	−0.111519
3		*−0.08016*	−0.109368	−0.114658
4			*−0.084978*	−0.116513
5				*−0.089986*

due to the built-in field effect. Under both strain conditions, it is found that the impact of a built-in field on polarization decreases with the increase of m, which is similar to the case without strain.

3.4 Strain controlling the transmission probabilities with different barrier thicknesses

According to the well-known WKB approximation, the transmission probability of electrons can be given as,

$$D(E_z) = \exp\left\{-\frac{2\sqrt{2}m_e^{1/2}\pi}{h}\int[\varphi(z) - E_z]^{1/2}\mathrm{d}z\right\} \quad (2)$$

where E_z is the kinetic energy of electrons in the z-direction, $\varphi(z)$ is the potential barrier along the z-axis, m_e is the effective electron mass, and h is the Planck constant. Our calculations focus on the transmission probability of electrons on the Fermi surface since it contributes most to the tunnel conductance, which can be expressed as,

$$D = \exp\left\{-\frac{2\sqrt{2}m_e^{1/2}\pi}{h}\int[\varphi(z) - E_f]^{1/2}\mathrm{d}z\right\} \quad (3)$$

where E_f is the Fermi energy of the supercell relative to the reference level which is equal to the electrostatic potential energy in our case. According to the bulk-plus-lineup method,[9,27]

$$\varphi(z) - E_f = E_g - (E_f - E_v) = E_g - [E_f - (V(z) + \Delta)] \quad (4)$$

where E_g is the band gap of ZnO and $V(z)$ is the reference level. Δ is the difference between the valence band edge (E_v) and the reference level, which can be determined in the bulk ZnO calculation.

 This journal is © the Owner Societies 2015

Published on 03 September 2015. Downloaded by Michigan State University on 19/01/2016 16:58:04.

Here, we would like to emphasize the importance of adding on-site Coulomb interaction in ZnO. Take the 'h_t' supercell with m = 2 free of strain for example. The Schottky barrier height (SBH) at the Au/Zn interface is estimated to be ~ -0.1 eV without on-site Coulomb interaction according to this method. GGA thus predicts an ohm contact at the Au/ZnO interface due to its underestimated band gap of ZnO ($\sim$0.92 eV), which is obviously inconsistent with experiments.[39,40] To overcome this problem, we adopt the GGA+U method to add on-site Coulomb interaction in ZnO. This method opens up the band gap of ZnO ($\sim$2.13 eV) and gives $\sim$1.0 eV SBH at the Au/Zn interface, which is very important to calculate the transport behavior of ZnO PTJs. Meanwhile, we have made a comparison between our results and the published results obtained by the Heyd–Scuseria–Ernzerhof screened hybrid density functional (HSE) method, given in the ESI,† and found that our results are reliable.

According to eqn (3) and ignoring the change in the effective mass of electrons with strain, the ratio of transmission probability on the Fermi surface by strain reversal can be expressed as,

$$D_+/D_- = \exp\left\{-\frac{2\sqrt{2}m_e^{1/2}\pi}{h}\left[\int_a^b(\varphi_+(z)-E_{f+})^{1/2}dz - \int_c^d(\varphi_-(z)-E_{f-})^{1/2}dz\right]\right\} \quad (5)$$

where the subscript '±' denotes tensile and compressive in-plain strain, and (b–a) and (d–c) are the corresponding potential barrier widths. Here, we define a parameter (in units of eV$^{1/2}$ Å) as,

$$B = \int_a^b(\varphi_-(z)-E_{f-})^{1/2}dz - \int_c^d(\varphi_+(z)-E_{f+})^{1/2}dz \quad (6)$$

and use it to evaluate the strain-tunability of the potential barrier. Therefore, it is also relevant to the ratio of transmission probability on the Fermi surface by strain reversal. According to eqn (4), B can also be given by,

$$B = \int_a^b\{E_{g-}-[E_{f-}-(V_-(z)+\Delta_-)]\}^{1/2}dz - \int_c^d\{E_{g+}-[E_{f+}-(V_+(z)+\Delta_+)]\}^{1/2}dz \quad (7)$$

The parameter B for 'h_t' PTJs with different m (ranging from 2 to 7) is calculated and shown in Fig. 5(d). One can surprisingly see that this parameter is almost linear as a function of barrier thickness. From this sense, it can be inferred that the ratio of transmission probability on the Fermi surface at different strained PTJs decreases exponentially with the barrier thickness, which implies that the thickness dependence of strain-tunability on the tunnel conductance of ZnO PTJs can be simply described by an exponential law.

The ultimate objective of this paper is to investigate the strain-tuned transport properties of ZnO PTJs with respect to ZnO thickness. The optimized 'h_t' supercell with different m (ranging from 2 to 7) is used to build the two-probe structures (ZnO PTJs) in the ATK package. A fully self-consistent NEGF method combined with first principles DFT calculations is adopted to study the transport properties of strained PTJs. The conductance of the TJs can be expressed by,[18]

$$G = G_0\sum T(E_f, k_{||}) \quad (8)$$

where $G_0 \equiv e^2/h$ is the quantum conductance and $T(E_f,k_{||})$ is the transmission probability of electrons on the Fermi surface with a transverse wave vector of $k_{||}$.The electrons on the Fermi surface mainly contribute to the conductance of ZnO PTJs, so we calculate k-resolved transmission probability on the Fermi surface (shown in Fig. 6). Note that the maximum transmission probability exists at the center of a two-dimensional Brillouin zone (which is a typical characteristic of direct tunneling[41]), and tends to shrink towards the center with the increase of m. It is found that the transmission probability under both strains (±3%) exponentially decreases with the increase of m. The transmission probability under 3% strain is always larger than that under −3% strain. Meanwhile, the transmission probability under −3% strain (T_-) decreases much sharply with respect to m than that under 3% strain (T_+), thus the ratio of transmission probability (T_+/T_-) increases with the increase of m. For example, when m equals 2, the maximal transmission probability of ZnO PTJs under 3% and −3% strain is 8.66×10^{-3} and 1.75×10^{-3}, respectively, and the ratio is $\sim$4.95. When m equals 6, the maximal transmission probability of ZnO PTJs under 3% and −3% strain is 1.21×10^{-8} and 7.78×10^{-11}, respectively, and the ratio reaches $\sim$155.27.

3.5 The tunnel conductance of PTJs with different barrier thicknesses under strain

Furthermore, based on NEGF-DFT calculations, the tunnel conductance (in units of Siemens) of ZnO PTJs with respect to barrier thickness m is calculated, as shown in Fig. 7. For all thicknesses we consider, the tunnel conductance of ZnO PTJs is larger under 3% strain than under −3% strain. This is possibly because ZnO PTJs under tensile strain have a lower and narrower potential barrier. Importantly, the tunnel conductance of ZnO PTJs under different strain still decreases exponentially with the increase of m. This is consistent with the previous analysis based on the classical WKB model (Fig. 5). The dependence of tunnel conductance on m of the ZnO PTJs thus does not follow the non-exponential law like in the case of FTJs.[17] Compared with FTJs, on the one hand, the polarization in the ZnO PTJs is much less nonlinear with the barrier thickness. The impact of barrier thickness on the potential barrier through the modification effect of polarization is small for the ZnO PTJs. On the other hand, the polarization in FTJs results from the atomic rumpling which has a strong impact on the interfacial bonding state and hence the tunnel conductance.[42] However, for ZnO PTJs, the interfacial bonding state changes much less significantly as the two polar ZnO surfaces does not show rumpling. In this sense, the impact of polarization on the tunnel conductance through the interfacial bonding is also very limited in ZnO PTJs. Therefore, the size dependence of tunnel conductance in the ZnO PTJ still obeys the exponential law. Additionally, the conductance

Published on 03 September 2015. Downloaded by Michigan State University on 19/01/2016 16:58:04.

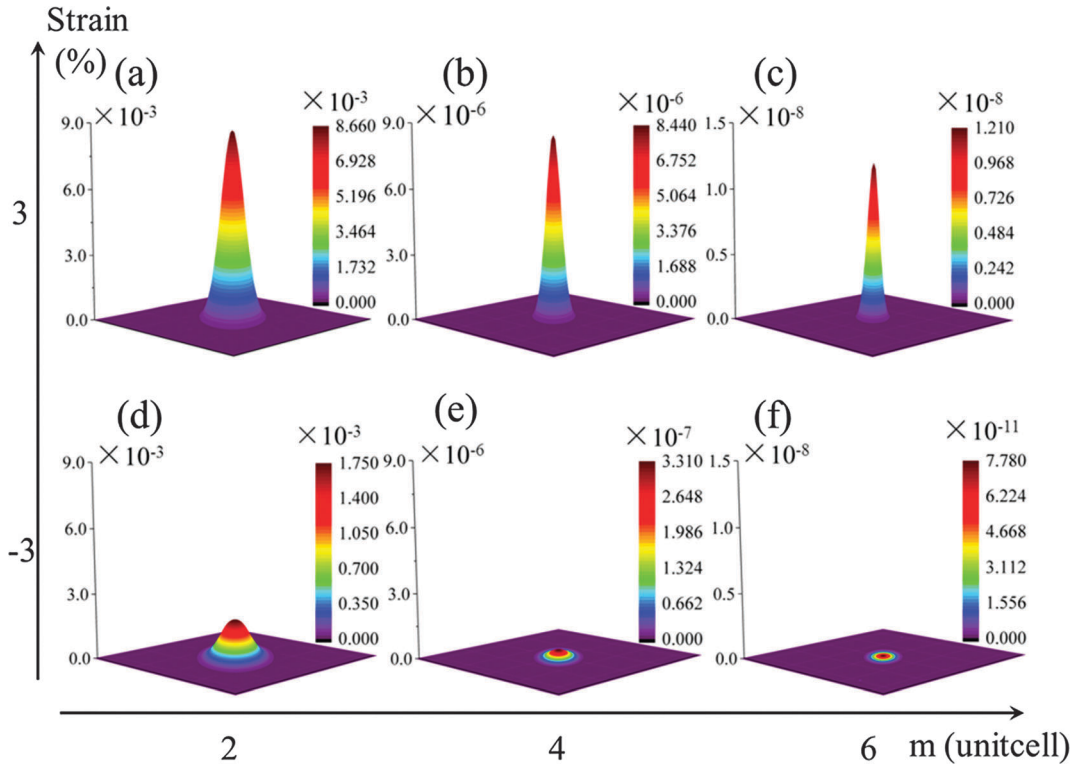

Fig. 6 The k-resolved transmission probability of 'h_t' ZnO PTJs on the Fermi surface with respect to m under ±3% in-plane strain.

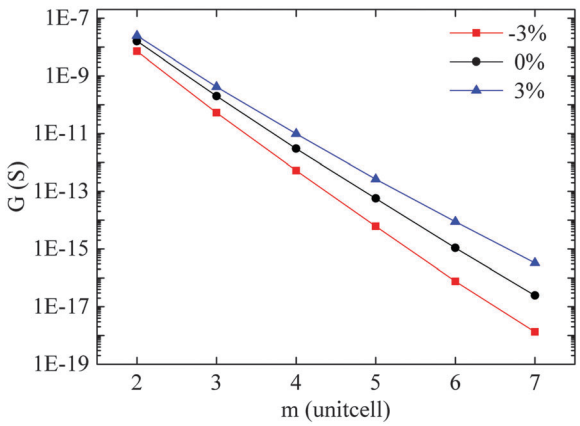

Fig. 7 The tunnel conductance (in units of Siemens) of 'h_t' ZnO PTJs with respect to m under strain −3%, 0% and 3%, respectively.

under −3% strain decreases much more sharply with respect to m than under 3% strain, which is similar to what has been found about k-resolved transmission probability.

3.6 The size-dependent amplification and difference in the tunnel conductance of PTJs by strain reversal

The ratio of tunnel conductance under −3% strain to that under no strain, *i.e.*, G_-/G_0, is calculated and shown in Fig. 8(a). This ratio is always smaller than 1 for all m, which means that compressive strain decreases the conductance of ZnO PTJs. Importantly, this ratio is found to exponentially decrease with the increase of m, which is the result of the exponential decrease of tunnel conductance. The smaller ratio with the increase of m means that the compressive strain tunability of the conductance of ZnO PTJs increases with the increase of m. Specifically, the ratio is ∼45% when m equals 7, and decreases to ∼5% when m equals 7. Similarly, the ratio of tunnel conductance under 3% strain to that under no strain, *i.e.*, G_+/G_0, is shown in Fig. 8(b). On the contrary, the ratio is always larger than 1, which means that the tensile strain enhances the conductance of ZnO PTJs. Importantly, the ratio increases exponentially (from ∼1.8 to ∼13.7) when m increases from 2 to 7, which implies that the tensile strain tunability of the ZnO PTJs also increases with the increase of m.

Finally, the thickness dependence of the tunnel conductance ratio G_+/G_- by the strain reversal is plotted in Fig. 9. It is observed that the ratio increases exponentially with respect to m. Specifically, the ratio increases from ∼3.4 to ∼243.1 when m increases from 2 to 7. This trend is similar to what is found in k-resolved transmission probability. According to eqn (5), the exponential increase of the ratio results from the linear increase of parameter B by strain reversal with respect to m. In this sense, the strain-tunable transport behavior of ZnO PTJs can be exponentially enhanced by the increase of barrier thickness. However, one should also notice that the difference in the conductance by strain reversal G_+–G_- decreases with the increase of barrier thickness. Therefore, there should still remain an optimum thickness of ZnO PTJs for the development of strain tunable applications considering the limited resolution of the current measurement in practice.

 This journal is © the Owner Societies 2015

Published on 03 September 2015. Downloaded by Michigan State University on 19/01/2016 16:58:04.

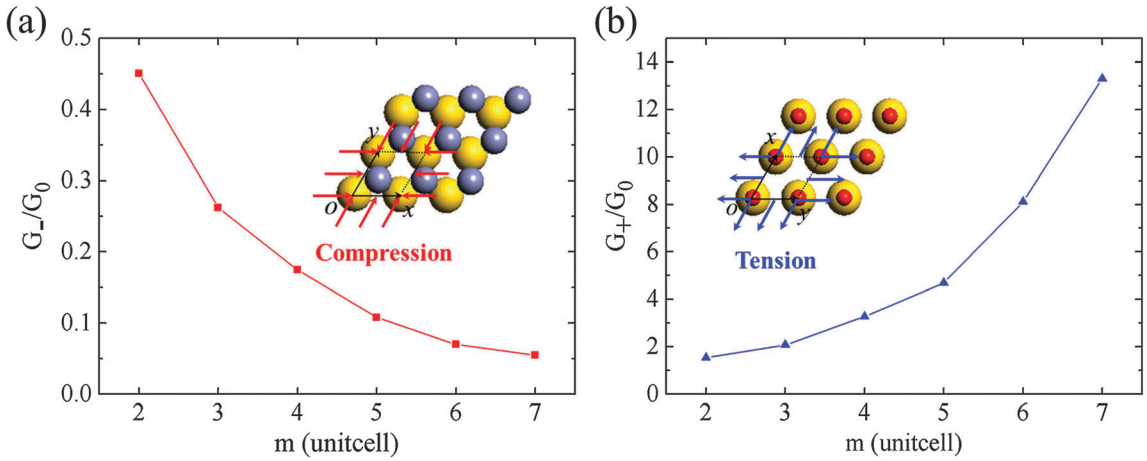

Fig. 8 The ratio of tunnel conductance of 'h_t' ZnO PTJs under (a) −3% and (b) 3% strain to that under 0% strain with respect to *m*. The insets show in-plane strain states.

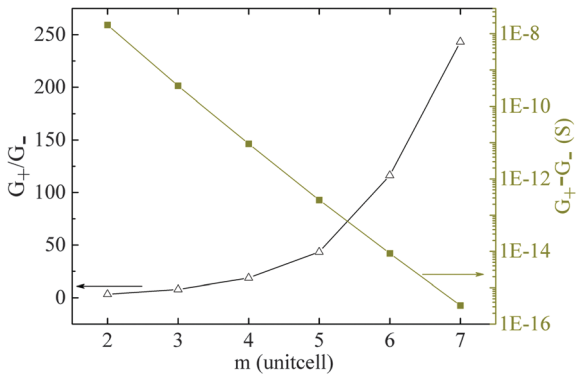

Fig. 9 The amplification (G_+/G_-, triangles) and the difference (G_+-G_-, squares) in the tunnel conductance of 'h_t' ZnO PTJs by strain reversal from −3% to 3% with respect to *m*.

4 Conclusion

Based on the first principles DFT calculations combined with the NEGF method, we have investigated the size-dependence of strain-tunability on the transport behavior of PTJs. Four types of ZnO PTJs with different interfacial bonding structures have been investigated. Interestingly, it is found that the cohesion energy of ZnO PTJs strongly depends on the interfacial bonding characteristics, especially at the O/Au interface. Additionally, the electric field in the barrier region is precisely determined by the difference in interfacial dipoles between the Au/Zn and O/Au interfaces. Based on the most energetically stable and unstable structures, we built ZnO PTJs with different ZnO barrier thicknesses. The electric field in the barrier is observed to decrease with respect to ZnO thickness, which is believed to mainly result from the decrease of the built-in field. Meanwhile, the spontaneous polarization is enhanced by the built-in field due to their same direction, and this enhancement decreases with respect to ZnO thickness. Then, the 'h_t' PTJs with different barrier thicknesses are studied under in-plane strain (±3%). In the framework of the WKB approximation, we characterize the difference in effective potential barriers by strain reversal. The parameter *B* is found to linearly increase with respect to ZnO thickness, which implies that the amplification of transmission probability by strain reversal exponentially increases with ZnO thickness. The *k*-resolved transmission probability on the Fermi surface of the PTJs clearly exhibits exponential decay with ZnO thickness under all kinds of strains, and decays sharply under compressive strain. Most importantly, the tunnel conductance of ZnO PTJs also decreases exponentially with respect to ZnO thickness. The tunnel conductance of ZnO PTJs under compressive strain decreases more quickly than under tensile strain, which leads to the result that by strain reversal the tunnel conductance ratio G_+/G_- increases exponentially with respect to ZnO thickness. On the whole, our simulations reveal that external in-plane strain can effectively tune the transport properties of ZnO PTJs, and the size-dependence of the strain tunability exhibits a simple exponential law. Our results regarding strain tunable transport behavior of piezoelectric tunnel junctions also provide basic ideas to develop novel piezoelectric and piezotronic nanodevices.

Acknowledgements

The authors acknowledge the financial support of the National Natural Science Foundation of China (No. 51172291, 11474363, 11232015, 11372361, and 11302268) and China Postdoctoral Science Foundation (2014M552267). Yue Zheng also thanks support from the Fundamental Research Funds for the Central Universities, Research Fund for the Doctoral Program of Higher Education, Fok Ying Tung Foundation, Science and Technology Innovation Project of Guangdong Provincial Education Department, and Guangdong Natural Science Funds for Distinguished Young Scholar and China Scholarship Council.

References

1 J. Zhou, D. Y. Gu, P. Fei, W. Mai, Y. Gao, R. Yang, G. Bao and Z. L. Wang, *Nano Lett.*, 2008, **8**, 3035–3040.

Published on 03 September 2015. Downloaded by Michigan State University on 19/01/2016 16:58:04.

2 L. Wang, Y. Kang, X. Liu, S. Zhang, W. Huang and S. Wang, *Sens. Actuators, B*, 2012, **162**, 237–243.
3 B. Kumar and S. W. Kim, *Nano Energy*, 2012, **1**, 342–355.
4 E. Lee, J. Park, M. Yim, Y. Kim and G. Hoo, *J. Appl. Phys.*, 2015, **106**, 023901.
5 P. Li, Q. L. Liao, Z. Zhang, Y. Zhang, Y. H. Huang and S. W. Ma, *Appl. Phys. Express*, 2012, **5**, 061101.
6 M. Akiyama, Y. Morofuji, T. Kamohara, K. Nishikubo, M. Tsubai, O. Fukuda and N. Ueno, *J. Appl. Phys.*, 2006, **100**, 114318.
7 Y. Zheng and C. H. Woo, *Nanotechnology*, 2009, **20**, 075401.
8 X. Luo, B. Wang and Y. Zheng, *ACS Nano*, 2011, **5**, 1649–1656.
9 G. H. Zhang, X. Luo, Y. Zheng and B. Wang, *Phys. Chem. Chem. Phys.*, 2012, **14**, 7051–7058.
10 G. Liu and C. W. Nan, *J. Phys. D: Appl. Phys.*, 2005, **38**, 584.
11 Y. Zheng, W. J. Chen, X. Luo, B. Wang and C. H. Woo, *Acta Mater.*, 2012, **60**, 1857–1870.
12 D. Cao, B. Liu, H. L. Yu, W. Y. Hu and M. Q. Cai, *Eur. Phys. J. B*, 2013, **86**, 504.
13 J. Wang, B. Völker, M. Kamlah and T. Y. Zhang, *Acta Mech.*, 2013, **224**, 1225–1231.
14 J. Junquera and P. Ghosez, *Nature*, 2003, **422**, 506–509.
15 H. Lu, X. Liu, J. D. Burton, C. W. Bark, Y. Wang, Y. Zhang and A. Cruverman, *et al.*, *Adv. Mater.*, 2012, **24**, 1209–1216.
16 Y. Liu, X. Lou, M. Bibes and B. Dkhil, *Phys. Rev. B: Condens. Matter Mater. Phys.*, 2013, **88**, 024106.
17 X. Luo, Y. Zheng and B. Wang, *J. Appl. Phys.*, 2012, **111**, 074102.
18 M. Brandbyge, J. L. Mozos, P. Ordejón, J. Taylor and K. Stokbro, *Phys. Rev. B: Condens. Matter Mater. Phys.*, 2002, **65**, 165401.
19 M. Y. Zhuravlev, R. F. Sabirianov, S. Jaswal and E. Y. Tsymbal, *Phys. Rev. Lett.*, 2005, **94**, 246802.
20 J. G. Simmons, *J. Appl. Phys.*, 1963, **34**, 1793–1803.
21 D. Bohm, *Quantum Theory*, Prentic Hall, Inc., Englewood Cliffs, New Jersey, 1951.
22 G. Kresse and J. Furthmüller, *Phys. Rev. B: Condens. Matter Mater. Phys.*, 1996, **54**, 11169–11186.
23 P. E. Blöchl, *Phys. Rev. B: Condens. Matter Mater. Phys.*, 1994, **50**, 17953.
24 J. P. Perdew, K. Burke and M. Ernzerhof, *Phys. Rev. Lett.*, 1996, **77**, 3865.
25 B. Himmetoglu, A. Floris, S. de Gironcoli and M. Cococcioni, *Int. J. Quantum Chem.*, 2014, **114**, 14–49.
26 G. Y. Huang, C. Y. Wang and J. T. Wang, *Comput. Phys. Commun.*, 2012, **183**, 1749–1752.
27 M. Peressi, N. Bingell and A. Baldereschi, *J. Phys. D: Appl. Phys.*, 2008, **31**, 1273–1299.
28 X. Ma, Y. Wu, Y. Lv and Y. Zhu, *J. Phys. Chem. C*, 2013, **117**, 26029–26039.
29 P. Erhart, K. Albe and A. Klein, *Phys. Rev. B: Condens. Matter Mater. Phys.*, 2006, **73**, 205203.
30 O. I. Malyi, V. V. Kulish, K. Bai, P. Wu and Z. Chen, *Surf. Sci.*, 2013, **611**, 5–9.
31 M. C. Muñoz, S. Gallego, J. I. Beltrán and J. Cerdá, *Surf. Sci. Rep.*, 2006, **61**, 303–344.
32 Y. Dong and L. Brillson, *J. Electron. Mater.*, 2008, **37**, 743–748.
33 J. Junquera, M. H. Cohen and K. M. Rabe, *J. Phys.: Condens. Matter*, 2007, **19**, 213203.
34 R. T. Tung, *Phys. Rev. B: Condens. Matter Mater. Phys.*, 2001, **64**, 205310.
35 J. Hoekstra and M. Kohyama, *Phys. Rev. B: Condens. Matter Mater. Phys.*, 1998, **57**, 2334–2341.
36 G. Singh-Bhalla, C. Bell, J. Ravichandran, W. Siemons, Y. Hikita, S. Salahuddin, A. F. Hebard, H. Y. Hwang and R. Ramesh, *Nat. Phys.*, 2010, **7**, 80–86.
37 C. Cazorla and M. Stengel, *Phys. Rev. B: Condens. Matter Mater. Phys.*, 2012, **85**, 075426.
38 R. Resta and D. Vanderbilt, *Physics of Ferroelectrics*, Springer, Heidelberg, Berlin, 2007.
39 Ş. Aydoğan, K. Çınar, H. Asıl, C. Coşkun and A. Türüt, *J. Alloys Compd.*, 2009, **476**, 913–918.
40 M. Asghar, K. Mahmood, M. Faisal and M. A. Hasan, *J. Phys.: Conf. Ser.*, 2013, **439**, 012030.
41 Y. Wang, J. Zhang, X. G. Zhang, H. P. Cheng and X. F. Han, *Phys. Rev. B: Condens. Matter Mater. Phys.*, 2010, **82**, 054405.
42 J. P. Velev, C. G. Duan, K. D. Belashchenko, S. S. Jaswal and E. Y. Tsymbal, *Phys. Rev. Lett.*, 2007, **98**, 137201.

 This journal is © the Owner Societies 2015